*Int. J. Heat Mass Transfer.* Vol. 27, No 12, pp. 2397–2413, 1984
Printed in Great Britain

0017-9310/84 $3.00 + 0.00


# Experiments on laminar flow and heat transfer in an elliptical duct

R. M. ABDEL-WAHED, A. E. ATTIA and M. A. HIFNI
Mechanical Engineering Department, University of Alexandria, Alexandria, Egypt.

(*Received* 17 *October* 1984 *and in revised form* 4 *May* 1984)

**Abstract**—Experiments were performed to study the laminar developing and fully developed flow and heat transfer inside an elliptical duct having an aspect ratio of 0.5. The working fluid was air and two thermal situations were investigated, the first with the duct at a uniform temperature and the second when the wall temperature distribution is linear in the axial direction and does not vary transversely. The hydrodynamic results are presented in the form of a sequence of velocity profiles on the major and minor axes, measured at axial locations extending from the duct entrance to the fully developed regime. The axial drop in the static pressure due to the combined effect of the flow development and wall friction is also reported. The extended length necessary for static pressure development, expressed as $x/Re\ D_h$, was found to be 0.0345. The thermal information depicts the temperature development in the duct entrance by a series of temperature profiles on the major and minor axes. The thermal results encompass as well the Nusselt number and the thermal entrance length in each of the above two thermal situations. To the author's knowledge, theoretical solutions for the hydrodynamic flow development in the entrance of elliptical ducts do not exist. The present experimental fully developed dimensionless velocity and friction factor were compared to the analytic value of L. N. Toa [On some laminar-forced-convection problems, *ASME J. Heat Trans.* **83**, 466–472 (1961)]. The percentage difference in the friction factor is 0.78%. The thermal development of the flow in the elliptical duct was studied analytically by N. T. Dunwoody [Thermal results for forced heat convection through elliptical ducts, *J. appl. Mech.* **29**, 165–170 (1962)] and V. Javeri [Analysis of laminar thermal entrance region of elliptical and rectangular channels with the Kantorowich method, *Wärme Stoffubert.* **9**, 85–98 (1976)] for the uniform and linear wall temperature ducts respectively. Both analyses assume either uniform or fully developed velocity profiles in the developing regime.

## INTRODUCTION

A VARIETY of modern engineering equipments incorporate virtually all kinds of noncircular flow passages. Literature on flow and heat transfer is obviously necessary for the design and optimization of such conduits. Some of these passages are not long enough for the flow to attain the fully developed regime. Furthermore, in many flow situations, the fluid is of such a high Prandtl number or the passage is of such a small hydraulic diameter that the flow pattern must be laminar. Outside flow across a slender elliptical tube experiences less pressure drop than over a circular one, and it is due to this advantage that numerous heat exchangers are nowadays built with elliptical tubes.

Using complex variables, closed form expressions for the laminar fully developed velocity of flow inside elliptical ducts were derived by Toa [1]. Similar results have been deduced elsewhere by [4–6]. Theoretical hydrodynamic solutions in the entrance region of elliptical ducts are not available. However, the total pressure drop due to flow development $K_\infty$, as well as the length needed for complete hydrodynamic development $L_e/Re\ D_h$ can be determined from the approximate methods devised by Lundgren *et al.* [7] and McComas [8], respectively. The fully developed friction factors of flow in elliptical ducts can be found in [7]. Chiranjivi and Ravi Prasad [9] measured friction factors in three different elliptical ducts having aspect ratios 0.25, 0.5 and 0.75 and the correlations contained an $L_e/D_h$ parameter. Shah and London [10] believe that the duct lengths in the experiments [9] are not long enough for the flow to achieve full hydrodynamic development and consequently the friction correlations [9] are valid neither for developing nor for fully developed flows. The experimental fully developed friction factors measured by Someswara Rao *et al.* [11] in an 0.25 aspect ratio duct deviate from the theoretical values by $\pm 10\%$.

On the energy transport side, Toa [1] analyzed the laminar fully developed heat transfer with internal energy generation in an elliptical duct receiving axially constant heat flux while its local transverse periphery is at a uniform temperature. Tyagi [12] extended the results of [1] to include viscous dissipation and reported closed form expressions for the $Nu_{H_1}$. The case of laminar fully developed heat transfer, with the simultaneously in the axial and circumferential directions uniform heat flux, was treated by Iqbal *et al.* [13], once with the conformal mapping and another with the variational analytic approaches. All published analytic solutions concerning the thermal entrance region of elliptical ducts assume either uniform or fully developed velocity profiles throughout the duct length. Dunwoody [2], assuming a fully developed velocity distribution, expressed by a double infinite series expansion the temperature development in the entrance of the elliptical duct. Applying the Galerkin method, Schenk and Han [14] checked the accuracy of the solution [2] and their results are in excellent

## NOMENCLATURE

| | |
|---|---|
| $D_h$ | duct hydraulic diameter |
| $f$ | friction factor |
| $K(x)$ | incremental pressure drop due to flow development |
| $L_e$ | entrance length |
| $Nu$ | Nusselt number |
| $P$ | pressure |
| $Pr$ | Prandtl number |
| $T$ | temperature |
| $Re$ | Reynolds number |
| $u$ | axial velocity |
| $x$ | axial coordinate |
| $y, z$ | transverse coordinates (major and minor) |

Greek symbols

| | |
|---|---|
| $\beta$ | temperature decay constant |
| $\rho$ | density |
| $\xi, \eta$ | elliptical cylinder transverse coordinates |
| $\phi$ | function defined, equation (5) |
| $\psi$ | $(T-T_w)/(T_0-T_w)$ |
| $\theta$ | $(T-T_w)/(\bar{T}-T_w)$ |
| $\lambda$ | eigenvalue, equation (5). |

Subscripts and superscripts

| | |
|---|---|
| $\bar{}$ | average value |
| 0 | at duct inlet |
| s | static |
| t | stagnation value |
| x | at axial location x |
| w | wall value. |

agreement with [2]. The fully developed Nusselt numbers $Nu_T$ can be obtained from the asymptotic values in [2]. Toa [15], with the variational calculus, derived a closed form expression for the variation of the fluid bulk temperature in the thermal entrance length of an isothermal elliptical duct. Employing the extended Lévèque method, Someswara Roa *et al.* [16] solved the thermal entrance problem in short ducts for either isothermal or constant heat flux boundaries. On the other hand, the method based on the Lèvêque theory and initially proposed by James [17] to predict the flow and heat transfer characteristics in the limiting geometries, was extended to evaluate the Nusselt number in isothermal ducts. James's approach [17] is in essence not different from that employed by [16], and therefore their mutual results agree excellently and also agree fairly well with [2] and [14]. Gilbert *et al.* [18] assumed a slug flow model to analyze laminar convection in the immediate vicinity of the entrance to an isothermal elliptical duct. Javeri [3] analyzed, using the Kantorowich method, the entrance problem with the wall temperature varying linearly in the flow direction while being, at any axial location, uniform peripherally.

From the foregoing literature survey, the need becomes evident for precise information regarding the separate hydrodynamic development as well as the simultaneous flow and temperature development in the entrance of elliptical ducts. The objective of the present research is not only to generate this information from a painstaking highly accurate experimental set up, but also to provide a base to check the approximations inherent in the solutions [2, 3, 18], due to idealization of the velocity distribution in the energy transport equation. Neither the experimental data [11], with the $\pm 10\%$ deviation in the friction factor, nor the correlations [9] can provide this datum.

## EXPERIMENTAL APPARATUS

This section describes the experimental set up used to study the hydrodynamic and thermal characteristics of laminar flow inside an elliptical duct having major and minor axes of 39.15 and 19.55 mm, respectively. The aspect ratio is therefore 0.49936 (approx. 0.5). The air circulation through the apparatus is of the induced draft type and is effected by a 0.55 Kw fan, Fig. 1. A 1.0 $\times$ 1.0 m stagnation aluminum plate is fixed at the entrance to the elliptical duct and simulates a semi-infinite plate which serves to eliminate any expected disturbances and flow asymmetries in the stream. The air leaving the downstream end of the elliptical duct enters a $20 \times 20 \times 30$ cm long parallelpiped box. The function of this box is to damp the flow oscillations arising from the intermittent action of the fan blades. The air mass flow rate is measured by a 19.25 mm diameter orifice meter, manufactured according to ASME specifications, and is incorporated in the 50.8 mm piping connecting the damping box to the suction fan. The flow rate, and consequently the Reynolds number, is controlled by a 50.8 mm gate valve placed ahead of the fan and is joined to it by a conic piping.

The 4 m test section, made of aluminium, was made using the extrusion method with a specially designed die. Figure 2 is a cross-sectional dimensioned drawing of the duct employed. The duct is formed from two symmetrical halves tied together with bolts and nuts. The two halves are aligned together with guide aluminum keys located in the longitudinal slot formed at the RHS of the duct block. The 28 heating cartridges, fitted to generate the desired thermal boundary, are embedded in longitudinal heaters' cavities (two at the top and two at the bottom). The heaters are divided electrically into seven groups. A group, occupying a given axial location, consists of four heaters, two cartridges in the top half of the duct and two in the bottom half. The four heating elements of a group are connected in series, and are energized independentally from other groups. The electrical energy input to a group is controlled by a variable resistance. The static pressure is measured at 25 axial locations. The static pressure taps drilled at the upper end of the minor axis are 0.7 mm in diameter, and are all checked microscopically for burrs at the edges. Thirty-two

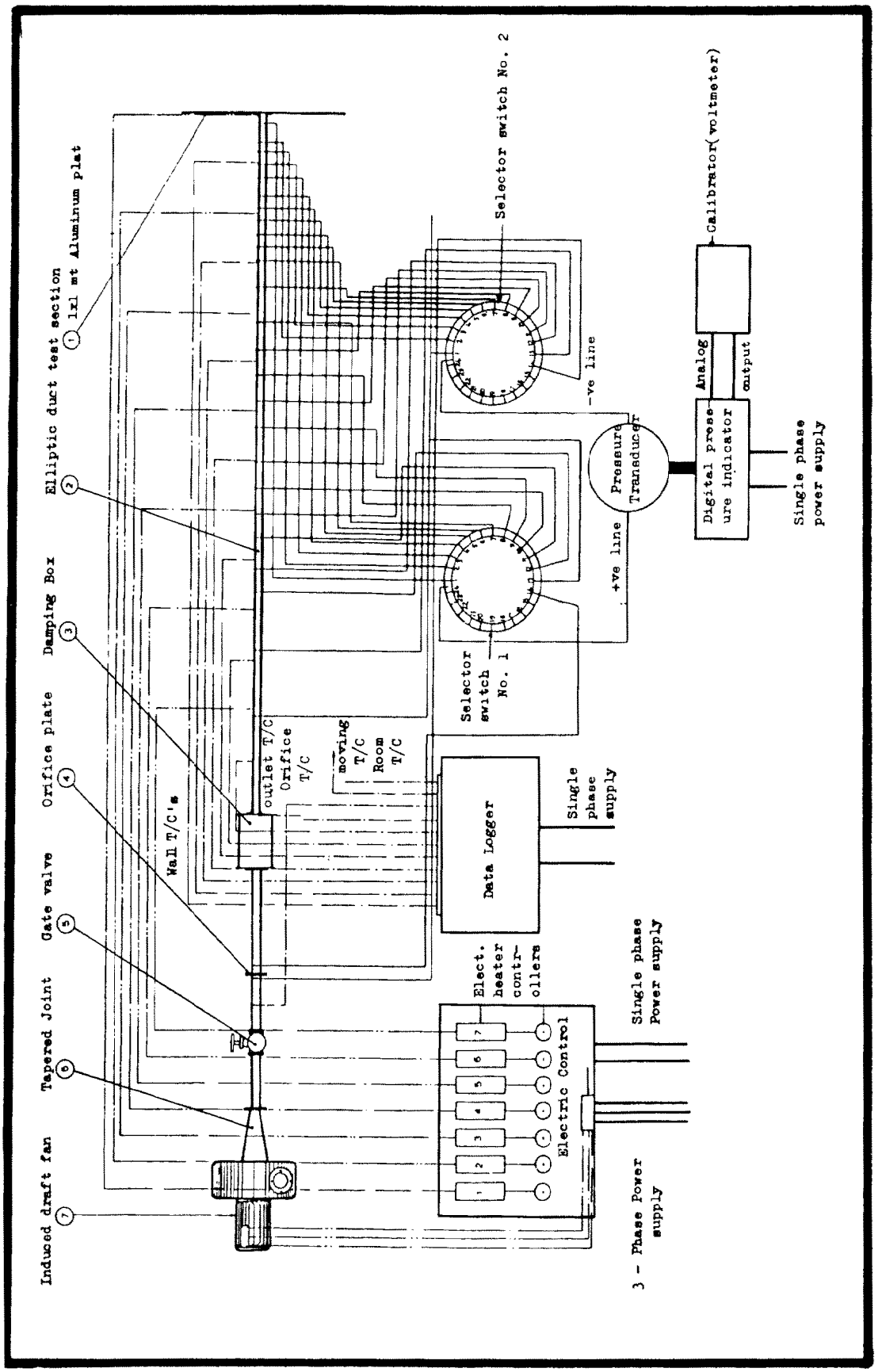


FIG. 1. Experimental arrangement.

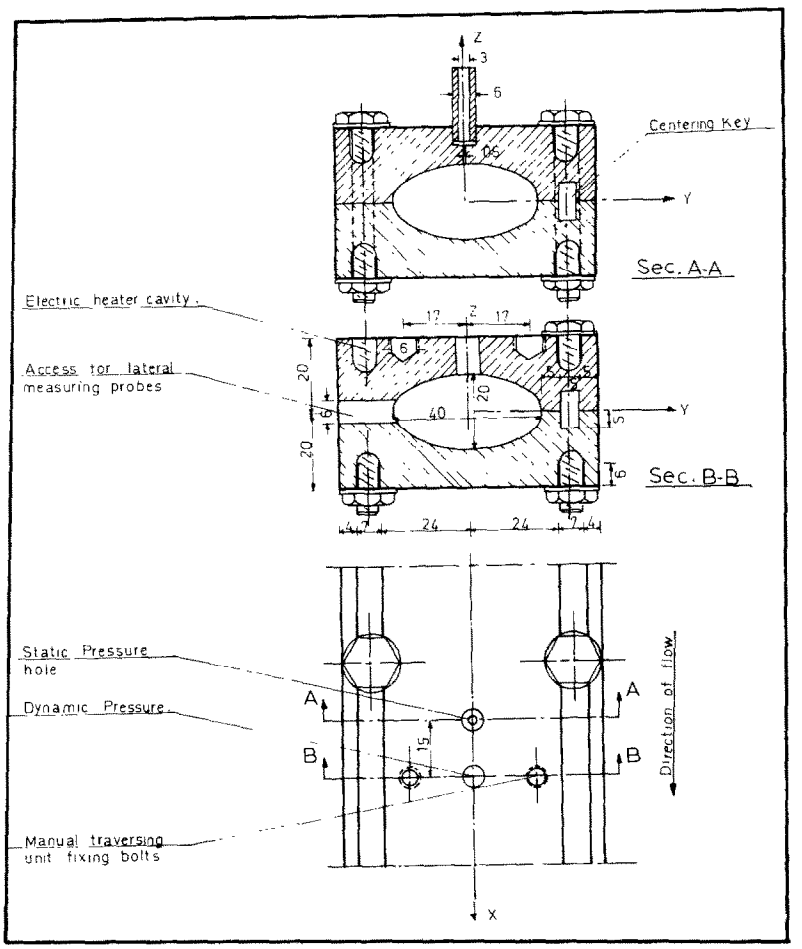


FIG 2. Elliptic duct cross-sectional view.

openings provide access for the velocity and temperature probes to the inside of the duct so that velocity and temperature distributions along the ellipse major and minor axes can be measured at 16 different axial locations. The openings' diameters are 6.25 mm, and not being in use, they are plugged by specially profiled copper inserts, each matched to a corresponding hole. Prior to the experimental runs, the inside elliptical surface of the test section, with the profiled plugs in place, is hand sanded and then polished using a lapping compound to ensure a perfectly smooth duct surface. The positions of the velocity probe holes are 15 mm downstream of the corresponding static pressure holes, the difference being the length of the foot of the L-shaped pitot tube utilized to measure the velocity. The pressure measurements are effected by a digital Baratron, manufactured by Setra systems, with a resolution down to 70 $\mu$m water head. The Baratron system is connected to two pressure selector switches with solenoid stepper drives to select between 24 channels. The pressure wiring diagram of Fig. 1 allows two alternatives for picking the static pressure distribution in the test section. Either the pressure difference between any two consecutive taps, or the pressure drop at any tap below the atmosphere can be determined. The velocity probe designed and fabricated for the measurement of the velocity field is of the stagnation type, having outside and inside diameters 1.15 and 0.9 mm, respectively, giving a diameter ratio of 0.78. The dimensions of the velocity probe used in the present investigation are so selected to be effective in reducing both the response time of the velocity sensor and the disturbances arising from the blocking of the flow passage by the probe. The ratio of the outside probe area to the elliptical duct area is only 0.173%. The excess dynamic head above the static pressure at any location in the duct is also read on the digital Baratron system. The velocity probe is mounted on a traversing mechanism which permits controlled travel normal to the wall. The position of the probe was determined by a vernier having a 0.05 mm resolution. An electric signal circuit is closed when the probe touches the duct wall. To avoid errors arising from the backlash in the lead screw of the traversing mechanism, the traverse of the probe is always made to begin from the wall side, opposite to where the traversing mechanism is mounted, towards the duct center line. As demonstrated in [19], for flow velocities corresponding to Reynolds numbers based on the probe outside diameter and less than 45, the transformation of the

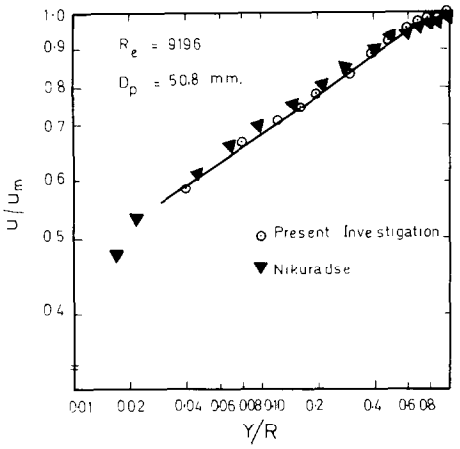


FIG. 3. Velocity measurement of turbulent air flow in a 50.8 mm round pipe.

dynamic head into pressure head at the probe mouth ceases to follow Bernoulli's equation and viscous forces play a role. Barker [19] incorporates this viscous effect in the evaluation of the flow velocities from Bernoulli's equation by proposing the following equation:

$$\frac{P_t - P_s}{\frac{1}{2}\rho u^2} = 1 + 4/Re_{\text{probe}}, \tag{1}$$

where $Re_{\text{probe}}$ is the Reynolds number based on the probe outside diameter. In order to establish the accuracy of the velocity measuring circuit, the velocity probe assembled with the traversing mechanism and connected to the Baratron system, is let to pick up the velocity distribution in the turbulent air flow inside a 50.8 mm diameter pipe. The recorded velocities, after being corrected if necessary according to equation (1), are compared with the experimental data of Nikuradse [20], Fig. 3. The velocity measurement accuracy will be discussed under Results.

Sensing of the temperature in the present experiments was accomplished by 18 AWG teflon-coated copper–constantan thermocouple wires. All thermocouples were calibrated to read temperature accurate to $\pm 0.1°C$. The temperature read-out and recording device is a multichannel Data Logger manufactured by Fluke. Seven thermocouples were embeded equidistantly in the duct upper wall. The function of these thermocouples is continuously to monitor the duct wall temperature and also, together with the heating elements in the wall, produce the required temperature boundary for the duct (isothermal or linear temperature). The temperature distribution inside the duct was measured by thermocouple slightly protruding from a 1.5 mm diameter stainless steel tube made to replace the velocity probe in the traversing aggregate. The temperature indication of the flow field thermocouple was corrected for errors arising from the heat exchange between the thermocouple ball and the duct wall by thermal radiation, convective heat loss from the thermocouple ball to the fluid stream, and also thermal conduction through the thermocouple leads and the tube itself. The details of the correction analysis are outlined in [21]. The exit of the elliptical duct is completely obstructed by a plane wire gauze made of pure copper, to which a copper–constantan thermocouple is welded. This system serves to measure the bulk temperature at the exit from the test section. Two more thermocouples were implemented to indicate the flow bulk temperatures at the inlet to the elliptical duct and in the circular tubing before the flow rate measuring orifice.

## RESULTS AND DISCUSSION

The presentation and discussion of results will be subdivided into two parts. The first is concerned with the hydrodynamic results, which encompasses the static pressure distribution and the flow velocity development. The second part concerns the thermal results, and deals with the temperature development in the flow field for the two cases of isothermal and linear wall temperature boundaries.

*Hydrodynamic results*

The hydrodynamic information about the flow in the elliptical duct is generated while the wall heaters are turned off.

*Static pressure distribution.* As the fluid stream enters the duct, the fluid layers adjacent to the duct wall experience retardation as a result of the friction with the duct wall. For a constant mass flow rate in the duct, the fluid particles outside this ensuing boundary layer have to speed up, and the axial drop in the fluid static pressure can best be described by:

$$\frac{P_0 - P_x}{\frac{1}{2}\rho \bar{u}^2} = \frac{x}{D_h Re}(f Re) + K(x) + 1, \tag{2}$$

where $P_0$ is the stagnation pressure at the entrance, $K(x)$ is a pressure function accounting for the pressure loss due to flow development in the distance between the duct entrance and a location $x$ in the duct, and its limiting value in the fully developed regime is $K(\infty)$. The laminar flow static pressure data is plotted in Fig. 4. From equation (2), the ordinate and the abscissa of the graph are selected to be $(P_0 - P_x)/\frac{1}{2}\rho\bar{u}^2$ and $(x/D_h Re)$ respectively. The static pressure experimental results are collected from 21 runs carried out at various flow Reynolds numbers ranging from 1118 to 3791. A least mean square technique is utilized to fair an average curve through the 297 experimental data points. As expected, the pressure gradient is maximum near the duct inlet and decreases monotonically with the downstream distance until it reaches a constant value. At this limit, the pressure field is said to have assumed its fully developed regime. The slope of the straight line part of the experimental pressure curve, $f\,Re$, equals 67.817. The theoretically predicted value [7], for a 0.5 aspect ratio duct, is 67.288. The experimental friction factor obtained is greater than the theoretical one by

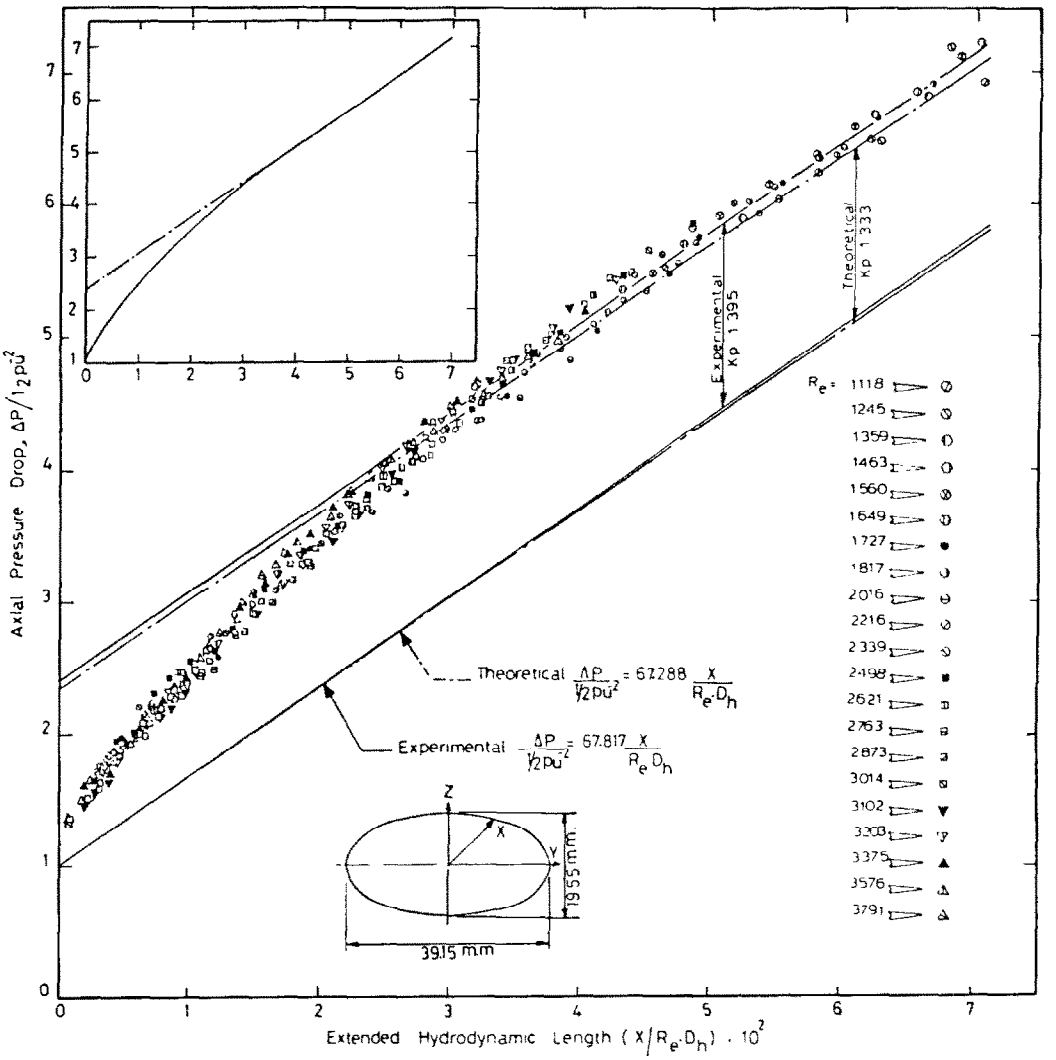


FIG. 4. Dimensionless static pressure drop in the entrance of the elliptic duct.

only 0.78%. In Fig. 4, through the point $(P_0 - P_x)/\frac{1}{2}\rho\bar{u}^2 = 1$ on the ordinate, are drawn two lines with slopes $f\,Re = 67.817$ and 67.288. The lines represent the experimental and theoretical solid wall friction as if fully developed flow starts right at the duct entrance. The vertical distance between the static pressure experimental data and the line $[67.817(x/Re\,D_h)+1]$ gives the pressure head expenditure on flow development in the entrance part, i.e. the function $K(x)$. In the LH upper corner of Fig. 4, the faired static pressure curve is redrawn in order to facilitate the utilization of this information. The solid line, passing through the pressure experimental data in the fully developed region and representing it, lies 1.395 units above the parallel line $[67.817(x/Re\,D_h)+1]$, which is the incremental pressure drop required for complete flow development, $K(\infty)$. The corresponding theoretical value from [7], for an elliptical duct with any aspect ratio, is 1.333. The experimental $K(\infty)$ is larger by 4.44%. The intersection of the convex and straight parts of the pressure distribution curve, obtained from the side graph of Fig. 4, locates the duct section where the flow has attained complete development. Within the accuracy of the figure, the extended length for complete static pressure development is 0.0345. The entrance length $L_e/Re\,D_h$ calculated theoretically by the approximate method devised by McComas [8], using the approximate analytic value $K(\infty)$ of 1.333 [7], is 0.02447. McComas [8] reports for the 0.5 aspect ratio elliptical duct an $L_e/Re\,D_h$ equals 0.02176. The difference between the two last values of $L_e/Re\,D_h$ is due to an error in evaluating the second complete elliptical integral in the expression of $f\,Re$. The tabulated results of $f\,Re$ and $L_e/Re\,D_h$ [10], corresponding to $K(\infty) = 1.333$, replaces the information in Table 2 of [8]. The method due to McComas [8] predicts smaller entrance lengths. The predicted $L_e/Re\,D_h$ value in the case of a circular tube [8] is 0.026, while the experimentally measured value by [22] is between 0.03 and 0.035. Another evidence of the low $L_e/Re\,D_h$ values of the method [8] is recognized from the comparison with the experimental data for the entrance lengths in the 5:1 and 2:1 rectangular ducts [23]. In a discussion of the paper [8], Professor Olson recommended that the

Table 1. Accuracy of velocity measurements

| $Re_D$ | 4488 | 5872 | 7063 | 7984 | 8824 | 9986 | 11190 |
|---|---|---|---|---|---|---|---|
| $u_m$(Orifice) | 6.037 | 7.858 | 9.283 | 10.506 | 11.582 | 13.090 | 14.593 |
| $u_m$(Probe) | 6.029 | 8.823 | 9.256 | 10.507 | 11.624 | 13.126 | 14.685 |
| % Diff. | −0.12 | −0.44 | −0.29 | 0.0029 | 0.036 | 0.27 | 0.63 |

experimental values for $K(\infty)$ are used instead of those calculated analytically by [7]. This gives $L_e/Re\,D_h$ equal to 0.0317 and 0.014 for the 2:1 and 5:1 rectangular ducts, respectively, and increases the entrance length for the circular tube from 0.026 to 0.028. The above modification due to Olson does partially improve the above analytical predictions of the $L_e/Re\,D_h$, but still leaves it below the experimental values. Inserting both the incremental pressure drop and the friction factor, determined from the present experiments on the 0.5 aspect ratio elliptical duct, in the expression introduced by [8], reduces the $L_e/Re\,D_h$ from 0.02477 to 0.02367. The experiments of [22] on the circular tube and the present one on the elliptical duct yield an entrance length around 0.035 vs an 0.025 value obtained by the improved method due to Olson. The approximate procedure outlined in [8] underestimates the entrance length by at least 25%.

*Velocity development in the entrance region.* The development of the velocity of flow in the entrance part of the 0.5 aspect ratio elliptical duct is represented by a series of velocity profiles measured along the major and minor axes at several axial locations from the duct entrance. To assess the accuracy of the velocity measuring probe with its pressure read-out device, as well as the flow rate measuring orifice, the elliptical test section is replaced by a 50.8 mm round pipe. The velocity probe is made to traverse transversely for the determination of the turbulent air flow fully developed velocity distribution in the round pipe. Figure 3 gives the velocity distribution corresponding to flow Reynolds number of 9196. For the sake of comparison, the results of Nikuradse [20] for flow Reynolds number equals 9200 and the distribution $u/u_m = (y/R)^{6.96}$, which is the least mean square fit to the present data, are produced on the same graph. There is a slight deviation, near the tube axis of the present data from the straight line. With a specified index $n$ for the velocity distribution $u/u_m = (y/R)^n$, it is possible to relate between the maximum and average velocities of turbulent flow in a round pipe [24]. The average velocity of flow in the pipe was first calculated from the measured mass flow in the orifice meter, and from which the center line velocity is evaluated. Under the same flow conditions, the maximum velocity is measured by the velocity probe. Table 1 compares the two values of the center velocity at different Reynolds numbers. Inspection of Table 1 reveals that the accuracy of measuring either the velocity or the flow rate is within ±0.5% of the measured variables. Figures 5a and b represent a succession of velocity profiles along the major and minor axes at different axial location from the elliptical duct entrance. The flow Reynolds number is 2229. The flow velocities corresponding to probe Reynolds number less than 45 were corrected for the viscous effects. The velocity distribution, whether on the major or minor axes, is flat near the duct inlet, and as a result of the growth of the wall boundary layer, becomes rounded as the flow proceeds downstream. For the purpose of comparison, the fully developed velocity profile [1], for the 0.5 aspect ratio elliptical duct, is presented in Fig. 5a. The agreement between the velocity experimental results and the analysis [1] is excellent. A cross-plot of the data presented in Figs 5a and b, with the transverse coordinates as parameters, reveals the course of development of the axial flow velocity along lines parallel to the duct axis and positioned at specific distances from the duct wall, Figs 6a and b. When the fluid enters the duct, the stream layers between $y/a = z/b = 0.9$ and the wall are immediately decelerated by the frictional forces set by the duct solid wall. In order to preserve constant flow rate, the inner layers have to speed up. In the dimensionless tube length $x/Re\,D_h$ less than 0.01, the influence of the wall shear stress continues to propagate gradually, through the just accelerated fluid layers, inwards towards the tube center, thus retarding flowing particles consecutively from $y/a = z/b = 0.8$ to 0.4, and accelerating the ever-shrinking potential core. The above adjustment in the axial flow field, evidently, necessitates mass replenishments be delivered continuously to the duct core and be extracted from the outer decelerating layers. Cross-fluid movements develop transverse vortices as those illustrated schematically in the insets of Figs 6a and b. The size and strength of a transverse vortex vary with the axial distance. Inspection of Fig. 6a, considering one-quarter of the duct only, reveals the existance of two such vorticies near the major axis, having their maximum intensities at $x/Re\,D_h = 0.015$ and 0.0266, respectively. From the graph also, it is seen that the effect of the transverse mixing can be felt quite a distance upstream the location of the maximum intensity of the respective vortex, so that beyond $x/Re\,D_h$ equals 0.012, the flow can no longer be classified as parabolic even in the proximity of the duct core. The strength of the first vortex, Fig. 6a, demolishes shortly after $x/Re\,D_h = 0.015$, and the flow along the major axis recovers from the retardation produced by the first transverse mixing. The fluid particles on the major axis attain thereafter higher velocities. The restored velocities are foreseen to lay on hypothetical curves 'A', Figs 6a and b. By hypothetical curves is meant presumed smooth curves faired between the velocity

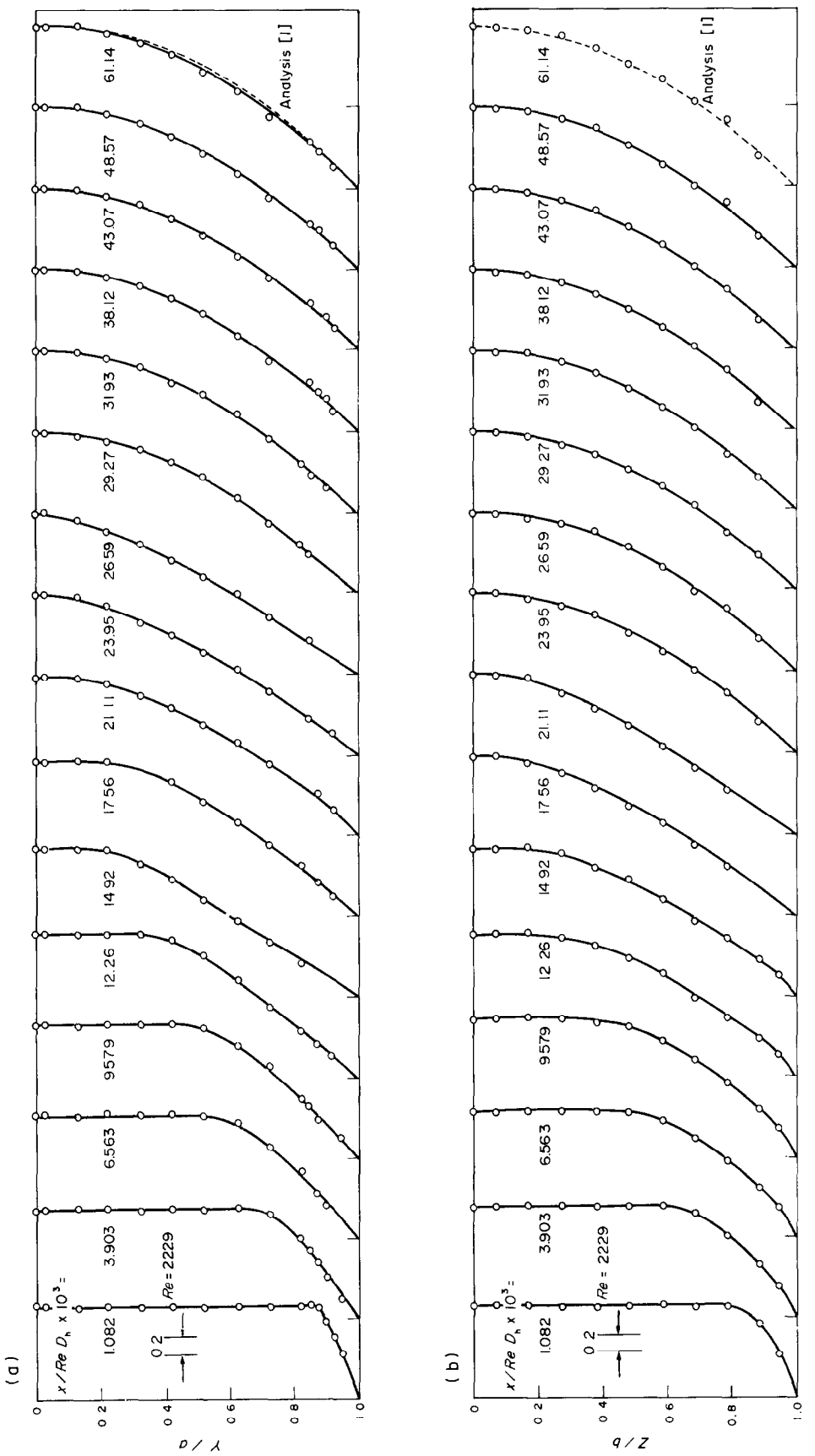


FIG. 5. Major (a) and minor (b) axis dimensionless velocity profiles ($u/\bar{u}$) in the entrance of the elliptic duct.

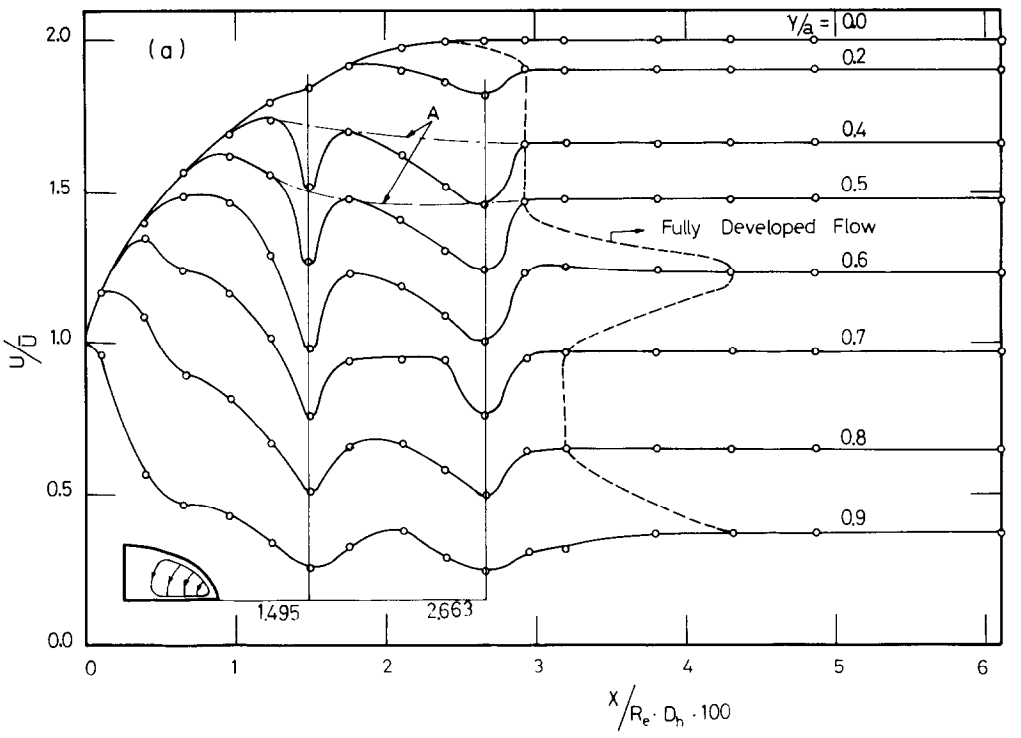


(a)

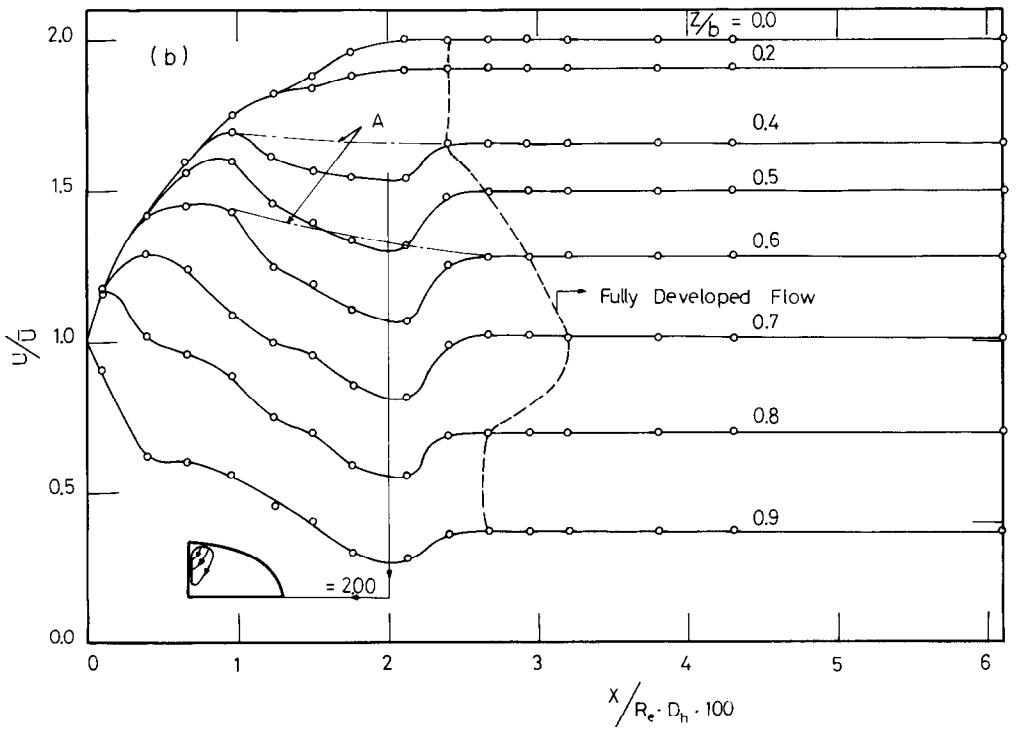


(b)

FIG. 6. Major (a) and minor (b) axis dimensionless velocity development ($u/\bar{u}$) in the entrance of the elliptic duct.

values of the accelerated particles ($y/a = z/b < 0.9$) near the duct entrance and the corresponding fully developed velocities. The curves may represent the deceleration of fluid particles solely due to a continuously connected friction from the wall while excluding the transverse mixing interruptions. The second transverse mixing on the major axis occurs just before the fully developed regime at $x/Re\,D_h = 0.0266$ and occupies a wider axial span than the one upstream at 0.015. The second vortex redistributes the flow across the duct, and the dashed lines on Figs 6a and b represent the axial locations where the various stream layers have reached velocities only 1% different from the fully developed values. The flow on the minor axis is subjected to a more flattered mixing vortex, similar to that indicated qualitatively on the inset of Fig. 6b. It extends over approximately the whole duct entrance length and has maximum intensity at $x/Re\,D_h \cong 0.02$. From Figs. 5 and 6, it is concluded that the fully developed velocity distribution on the major and minor axes have been attained after $x/Re\,D_h = 0.0431$ and 0.033, respectively. Some of the velocities, at certain locations in the duct, attain constant values before others. In other words, there is specific developing length corresponding to every transverse position in the duct. This statement does not contradict with the mass conservation of the flow. An example can be quoted from the observation of the variation of the center line velocity. The wall effect, through the shorter track along the minor axis, determines and fixes the value of the duct center velocity in axial distance $x/Re\,D_h < 0.024$, On the ellipse major axis, in the tube length $0.04324 > x/Re\,D_h > 0.024$, Fig. 6a demonstrates a further development of the flow velocity in the transverse distance $0.8 > y/a > 0.2$. In this research, it was decided to select the developing entrance length for the complete development of the velocity as the axial distance required for the flow velocity to attain a uniform value on every point on both the major and minor axes.

The foregoing comparison between either the experimental fully developed friction factor or the fully developed velocity profiles, along the major and minor axes, and the closed form analytical expressions for the above characteristics provides confidence in the accuracy of the present results. The approximate method [7] determines the incremental pressure drop in elliptical tubes with reasonable accuracy. The procedure due to McComas [8], to estimate approximately the entrance length in noncircular tubes, can predict with serious deviations only the length for hydrostatic pressure development and not the length for the velocity development. In some situations of flow inside noncircular tubes, it is possible that complete velocity development can be achieved on one axis of symmetry before the other.

*Heat transfer results*

In this section the heat transfer results of the laminar flow in the elliptical duct are presented. As previously mentioned two thermal boundary conditions were investigated, namely, the isothermal and the linear wall temperature boundaries. For each case, the course of development of the transverse temperature distribution in the thermal entrance length of the duct up till the thermally fully developed regime is presented. The fully developed Nusselt number and the thermal entrance length are also determined.

*The uniform wall temperature duct.* Figure 7a and b are plots of the experimental axial variation of the dimensionless temperature distribution, $\theta$, along the major and minor axes of the ellipse for the case of laminar flow with a Reynolds number 1718. The duct wall and the entering air temperatures are 53.4 and 30.6°C, respectively. Generally for an internal flow in a duct, the axial bulk temperature gradient is connected to the average circumferential wall gradient by:

$$\frac{d\bar{T}}{dx} = \frac{4}{Re\,Pr}\frac{1}{p}\oint_p \left(\frac{dT}{dn}\right)_w dp. \tag{3}$$

Specifically, if a thermally fully developed regime is established inside an 0.5 aspect ratio elliptical duct, the total average wall gradient in the RHS of equation (3) could be replaced by the arithmetic average of the wall gradients at the ends of the major and minor axes, so that:

$$\frac{d\bar{T}}{dx} = \frac{4}{Re\,Pr}\frac{1}{2}\left[\left(\frac{\partial T}{\partial y}\right)_{y=a} + \left(\frac{\partial T}{\partial z}\right)_{z=b}\right]. \tag{4}$$

The copper wire gauze mounted at the outlet of the elliptic duct, with a sensing thermocouple attached to it, determines the bulk temperature at the duct exit. The experimental wall temperature gradients near the duct exit are used with equation (4) to determine the local upstream bulk temperature. This procedure is followed between the successive measuring stations and is continued even in the developing length until the inlet air temperature is finally found. The difference between the thus calculated inlet air temperature and its directly measured value did not, in several runs, exceeds 0.2 K. Next, local heat transfer coefficient, based on the above bulk temperature, was evaluated.

Near the duct entrance, the dimensionless temperature profile $\theta$ (Fig. 7) is flat and becomes rounded as we proceed downstream in the duct. On the same graphs, the analytical prediction of Dunwoody [2] for the development of the temperature distribution in the entrance region of an isothermal elliptical duct is also plotted. The analysis [2] assumes a fully developed velocity profile throughout the duct and expresses the three-dimensional temperature distribution, in terms of elliptical coordinates, by the following equation:

$$\psi(\zeta, \eta, x/Re\,Pr\,D_h) = \sum_{m,n} A_{m,n} \times \phi_{m,n}(\zeta, \eta) \exp\left(-\frac{\lambda_{m,n} x}{D_h\,Re\,Pr}\right), \tag{5}$$

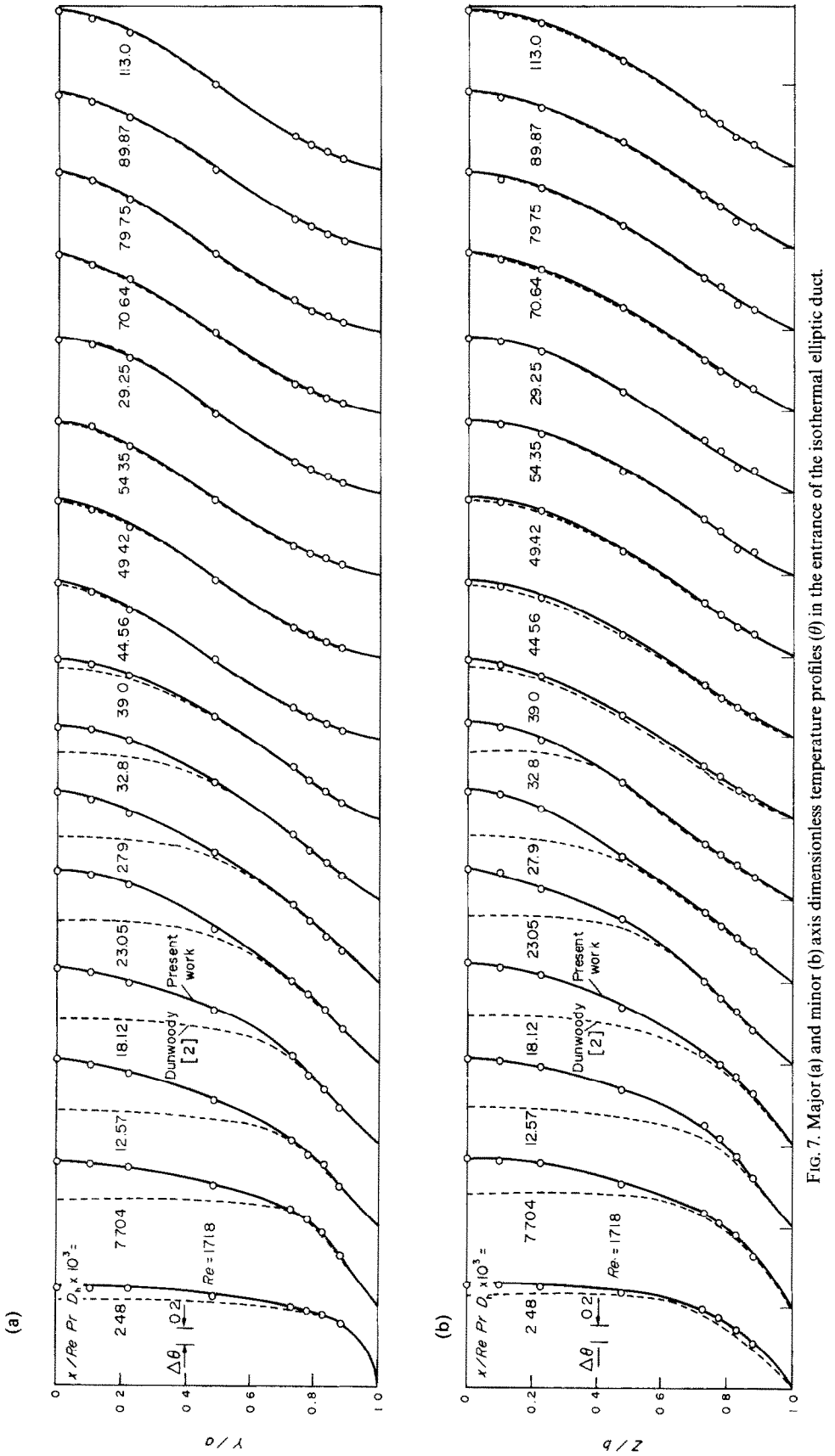


FIG. 7. Major (a) and minor (b) axis dimensionless temperature profiles ($\theta$) in the entrance of the isothermal elliptic duct.

where

$$\phi_{m,n} = \sum_{p,q} a_{p,q}^{m,n} \sin p\left[\frac{\pi}{2}\left(\frac{\zeta}{\zeta_0}+1\right)\right]\cos(q\eta)$$

$$m,p = 1,3,5,\ldots; \quad n,q = 0,2,4,\ldots.$$

Dunwoody [2] reports, for the 0.5 aspect ratio elliptical duct, only the parameters of the first group in the expansion (5). In order to attain a better comparison, the next two groups in the expansion were generated. The coefficients of the eigenfunctions and the eigenvalues are listed in the Appendix. Inspection of Figs 7a and b reveals that close to the duct entrance the analytical dimensionless temperature $\theta$ values are smaller than those measured experimentally. The difference is largest at the duct core, and as the flow velocity develops the analytical profile approaches the experimental one, until they finally coincide at $x/Re\,Pr\,D_h \simeq 0.05$. The coincidence between the two temperature profiles in the fully developed regime is remarkably good. It is most probable that the difference is due to the simplification involved in the analysis [2] by assuming a fully developed velocity distribution right from the duct inlet. Hence, it can be claimed that, it is this difference which reflects the degree of approximation in the analysis [2], if the latter is made to replace a rigorous simultaneous hydrodynamic and thermal developing solution. The axial variation of the local Nusselt number at the ends of the major and minor axes is plotted in Fig. 8 for both the present experimental data and the analysis [2]. The local Nusselt number decreases montonically from the duct inlet to its constant value in the fully developed regime. The local Nusselt at the end of the minor axis is always larger than at the end of the major. As expected, the Nusselt numbers from [2] are below those measured in the present experiments. The local Nusselt values of the analysis [2] and the present experiments coincide excellently in the fully developed regime. To complete the task, it is useful to investigate the effect of the idealizations included in the approximate theoretical analysis [18]. Gilbert *et al.* [18] assume slug flow in the duct and further neglect the heat conduction in the direction of the major axis relative to that in the minor direction. The Nusselt numbers of [18], plotted in Fig. 8, are much lower than those of the present experiments. They are even below the Nusselt values [2], derived with fully developed profiles. This goes against the normal expectations, and the reason could be due to the second idealization postulated above. The local Nusselt values [18] do not decrease to the fully developed local values but approach the zero value asymptotically. From the characteristics of thermally and hydrodynamically fully developed flow in an isothermal duct of uniform cross-section, it is possible to relate the two temperatures of the fluid at the same transverse location but axially apart by $\Delta x$ by the following equation:

$$(T - T_w)_{x+\Delta x} = (T - T_w)_x \exp(-\beta \Delta x), \tag{6}$$

where $\beta$ is a thermal decay constant. Furthermore, the fully developed Nusselt number can be evaluated if the decay constant $\beta$ is known:

$$\frac{4\,Nu_T}{Re\,Pr} = \beta/\left(\frac{1}{D_h}\right). \tag{7}$$

Hence, in order to determine experimentally the fully

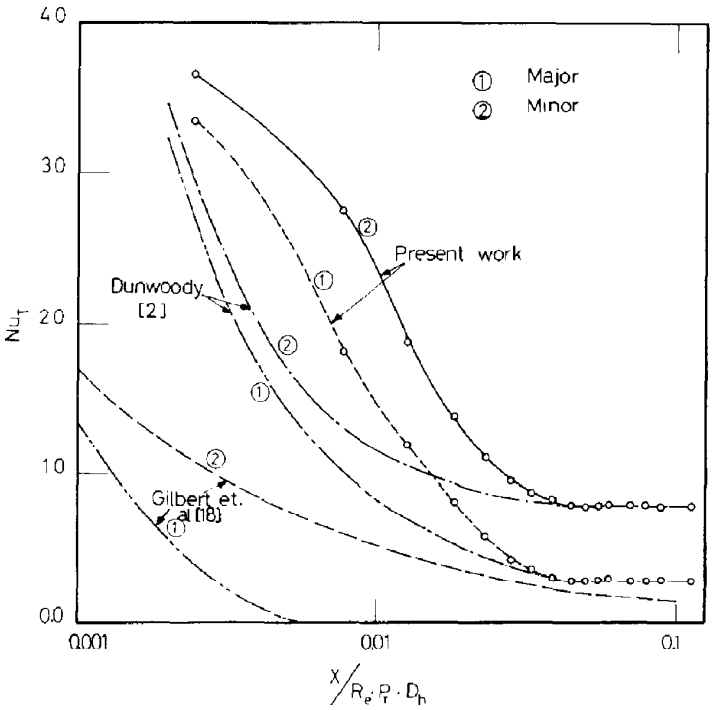


FIG. 8. Entrance local Nusselt number of the isothermal elliptic duct.

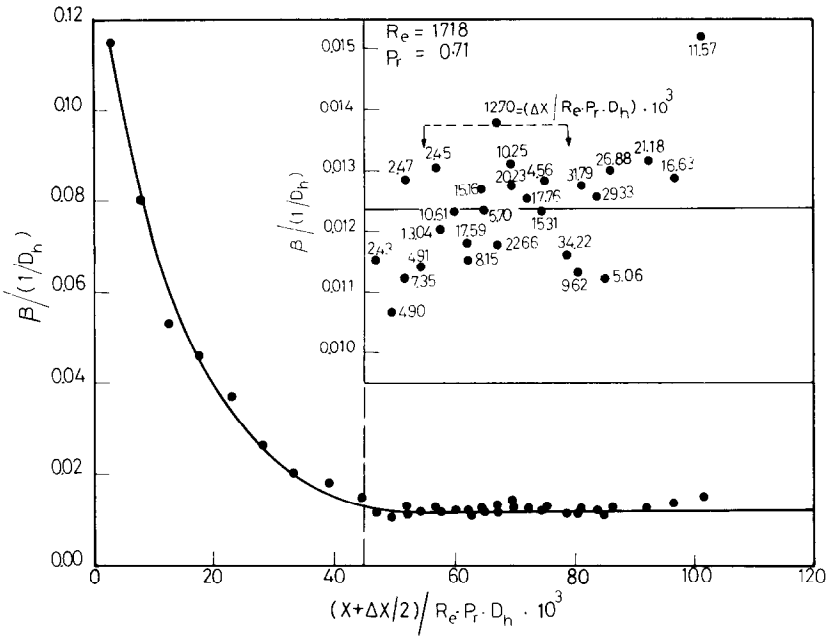


FIG. 9. Temperature decay constant in the fully developed regime of the isothermal elliptic duct.

developed Nusselt number $Nu_T$, it is sufficient to measure two temperatures at the same transverse position in the duct and distant $\Delta x$ in the fully developed regime and use equations (6) and (7) to calculate $\beta$ and $Nu_T$ successively. This approach is much simpler, from the practical point of view, than thermally insulating the duct and measuring the heat flux input and the rise in the bulk temperature with the duct axis. In other words, the fully developed Nusselt number, for an isothermal duct with uniform but arbitrarily shaped cross-sectional area, can be measured by a single thermocouple probe traversing the temperature field axially while preserving a fixed transverse location in the duct. This method was conveniently used here to evaluate experimentally the $Nu_T$ in the 0.5 aspect ratio elliptical duct. The value of $\beta$ calculated from any two measured temperatures at $x$ and $x+\Delta x$, is specified to be at $x+(\Delta x)/2$. Figure 9 represents experimental values of the dimensionless decay constant $\beta/(1/D_h)$, calculated from matching temperatures at different axial locations in both the developing and fully developed sections of the duct. The dimensionless decay constant decreases monotonically from the duct entrance till it assumes a fixed magnitude in the fully developed regime. The top part of Fig. 9 is an expanded view of the 27 $\beta/(1/D_h)$ data points in the thermally fully developed range. The abscissa of the figure is the axial location $(x+\Delta x/2)/Re\ Pr\ D_h$) of the intermediate point midway between two stations, $\Delta x/Re\ Pr\ D_h$ apart, and whose temperatures were used to evaluate $\beta/(1/D_h)$. The number adjacent to each dark circle in the top part of Fig. 9 is the distance $\Delta x/Re\ Pr\ D_h$. The average value of the points in the top view is 0.01237 and the corresponding $Nu_T$ is 3.745. The theoretically predicted value [2] is 3.729, which differs by 0.43% from the present experimental value. The thermal entrance length was determined when the calculated value of the decay constant $\beta$ begins to deviate from its asymptotic value in the fully developed regime. The thermal entrance length $L_e/Re\ Pr\ D_h$ found from the data in Fig. 9 is 0.04699. This value is not far away from the one (0.04942) at which the dimensionless profiles of [2] and the present work merge.

*The linear wall temperature duct.* This boundary can be met in counterflow heat exchangers. Figures 10a and b illustrate the corrected measured dimensionless temperature profiles, on the major and minor axes, while developing from the duct entrance down to the thermally fully developed regime. In this experiment, the duct wall temperature rose linearly from 35.11°C at the duct inlet to a maximum of 51.45°C near the duct exit. The entering air temperature and the flow Reynolds number were 26.3°C and 1960, respectively. The dimensionless temperature profile, as expected, is flat at duct entrance, becomes rounded in the downstream direction. Javeri [3], using the variational calculus, studied the entrance wall temperature duct problem, and used the Runge–Kutta method to solve the resulting set of ordinary differential equation. For better accuracy, the solution of the same set of ordinary differential equations [3] is obtained by the present authors using the matrix inversion technique. In [3], two limiting velocity idealizations were assumed throughout the duct length, the fully developed and the slug or uniform profiles. For the sake of evaluating the results of [3], the analytic results obtained by the matrix inversion method are presented on Figs 10a and b. The slug flow model is always away from the present experimental data, and continues to be so even in the hydrodynamically and thermally fully developed regimes. The fully developed model is a better approximation than the slug flow one. The experi-

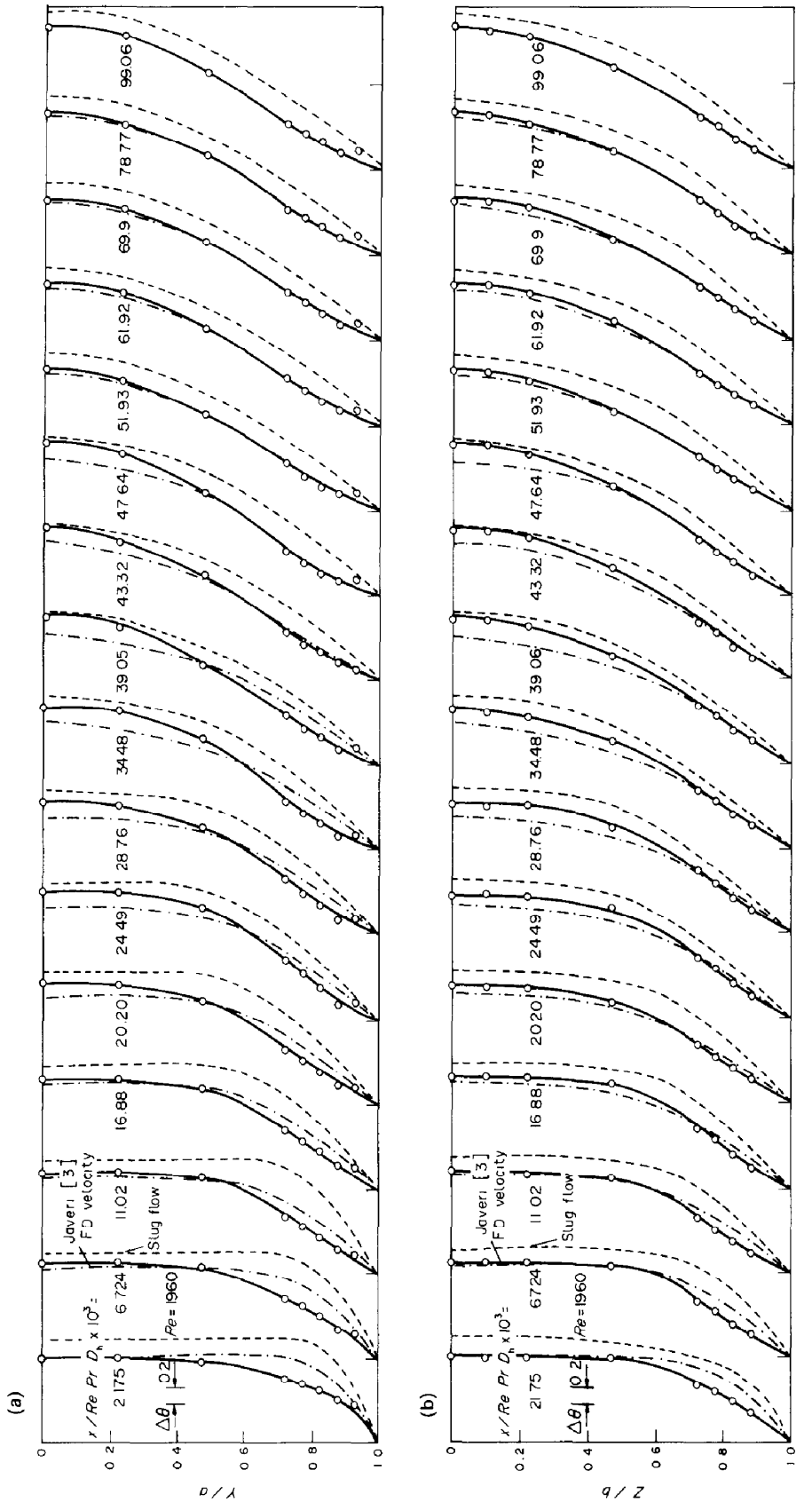


FIG. 10. Major (a) and minor (b) axis dimensionless temperature profiles ($\theta$) in the entrance of the linear wall temperature elliptic duct.

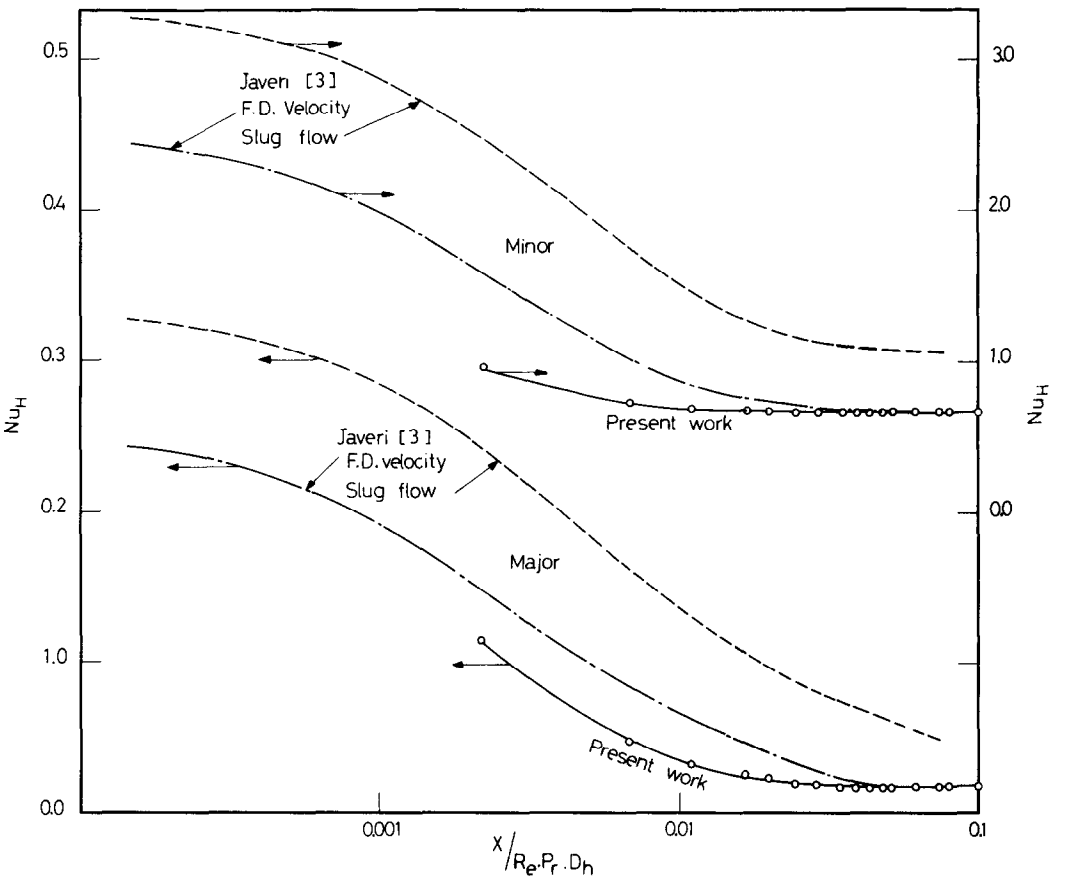


FIG. 11. Entrance local Nusselt number of the linear wall temperature elliptic duct.

mental dimensionless temperature profile and the fully developed model solution [3] coincide at $x/Re\ Pr\ D_h = 0.09906$. Before we turn to the heat transfer results, it is important to notice the temperature experimental data on the major axis at $y/a = 0.925$. The temperature profile at this location on the major axis experiences a sudden increase. This experimental observation does not exist in the case of the measurement on the minor axis. Hence, the reasoning that an instrumental error might be the cause is excluded, and axial heat conduction near the duct wall may be significant. In the hydrodynamically and thermally fully developed regime, it is well known that the fluid temperature distribution for the linear wall temperature and constant wall axial heat flux with uniform transverse temperature boundaries are similar. The comparison of the analytic fully developed temperature profile [1], for the constant heat flux boundary, with the present experimental data revealed excellent agreement, to the extent that the profile [1] cannot be distinguished from the fully developed experimental data in Figs 10a and b.

The development of the experimental local Nusselt number, at the ends of the major and minor axes, is plotted in Fig. 11, together with the analytic results of Javeri [3]. The two models used by Javeri [3] predict higher values of the Nusselt number. As stated before, the slug flow model gives a larger deviation than the fully developed model. The Nusselt number at either axis assumes its constant fully developed value at $x/Re\ Pr\ D_h = 0.094$, which is close to the location where the analytic solution [3] coincides with the experimental results.

In the case of the fully developed linear wall temperature boundary, the fluid bulk temperature axial gradient is constant and is the same as the wall temperature gradient, and the axial temperature gradient at any point in the fluid. The value of $\beta$ in equation (7), could be determined from:

$$\beta = -\frac{1}{(\bar{T}-T_w)}\frac{d(\bar{T}-T_w)}{dx}. \tag{8}$$

The value of the derivative in equation (8) is known from either the wall gradient or the fluid axial temperature gradient, and it remains to know the local value of the bulk temperature in order to decide upon the magnitude of $\beta$. As before the wire gauze at the duct outlet provided the bulk temperature at exit, and with the knowledge of the linear bulk temperature axial gradient in the fully developed regime, bulk temperatures in the fully developed part were determined. The procedure outlined in the isothermal duct experiments was then adopted to calculate bulk temperatures throughout the duct. Comparison of the fully developed bulk temperatures from the two methods showed excellent agreement. The above

procedure yielded an air temperature at inlet higher than the actual value by only 0.4 K. Ten values of $\beta$ in the fully developed region were calculated and the average $\beta$ was found to by 0.013196 which corresponds to a fully developed Nusselt number of 4.5587. The theoretical fully developed Nusselt number [1] for a constant heat flux duct, $Nu_H$, is 4.5575 and the difference is only 0.02%.

## CONCLUSION

The accurate measurements of the flow and heat transfer in an 0.5 aspect ratio elliptical duct revealed the need for a better analytical solution in the entrance section of such ducts. The existing approximate solutions predict the trend in the flow and heat transfer characteristics in the entrance portion but do not yield this information quantitatively accurate.

## REFERENCES


1. L. N. Toa, On some laminar forced-convection problems, *ASME J. Heat Trans.* **83,** 466–472 (1961).
2. N. T. Dunwoody, Thermal results for forced heat convection through elliptical ducts, *J. Appl. Mech.* **29,** 165–170 (1962).
3. V. Javeri, Analysis of laminar thermal entrance region of elliptical and rectangular channels with the Kantorowich method, *Warme Stoffubert.* **9,** 85–98 (1976).
4. J. G. Knudsen and D. L. Katz, *Fluid Dynamics and Heat Transfer.* McGraw-Hill, New York (1958).
5. H. L. Dryden, F. D. Murnaghon and H. Bateman, *Hydrodynamics,* Bulletin No. 84, pp. 197–201. Comm. Hydrodyn., Div. Phys. Sci., Natl. Res. Counc., Washington D.C., 1932, reprinted by Dover, New York (1956).
6. F. S. Shih, Laminar flow in axisymmetric conduits by a rational approach, *Can. J. Chem. Engng.* **45,** 284, (1967).
7. T. S. Lundgren, E. M. Sparrow and J. B. Starr, Pressure drop due to the entrance region in ducts of arbitrary cross-section, *J. Basic Engng.* **86,** 620–626, (1964).
8. S. T. McComas, Hydrodynamic entrance lengths for ducts of arbitrary cross-sections, *J. Basic Engng* **89,** 847–850 (1967).
9. C. Chiranjivi and A. Ravi Prasad, Study of laminar flow friction in elliptical conduits, *Indian J. Technology* **12,** 87–90 (1974).
10. R. K. Shah and A. L. London, *Laminar Flow Forced Convection in Ducts,* pp. 247–252. Academic Press, New York (1978).
11. S. Someswara Rao, D. Changal Raju and M. V. Ramana Rao, Pressure drop studies in elliptical ducts, *Indian J. Technol.* **13,** 6–11 (1975).
12. V. P. Tyagi, Laminar forced convection of a dissipative fluid in a channel, *J. Heat Trans.* **88,** 161–169 (1966).
13. M. Iqbal, A. K. Khatry and B. D. Aggarwala, On the second fundamental problem of combined free and forced convection through vertical noncircular ducts, *Appl. Sci. Res.* **26,** 183–208 (1972).
14. J. Schenk and B. S. Han, Heat transfer from laminar flow in ducts with elliptical cross-section, *Appl. Sci. Res.* **17,** 96–114 (1967).
15. L. N. Toa, Variational analysis of forced heat convection in a duct of arbitrary cross-section, *Proc. Int. Heat Trans. Conf., 3rd,* AICHE, New York 1, 56–63 (1966).
16. S. Someswara Rao, N. C. Pattabhi Ramacharyulu and V. V. G. Krichnamurty, Laminar forced convection in elliptical ducts, *Appl. Sci. Res.* **21,** 185–193 (1969).
17. P. A. James, Forced convection heat transfer in narrow passages, *Can. J. Chem. Engng,* **48,** 330–332 (1970).
18. D. E. Gilbert, R. W. Leay and H. Barrow, Theoretical analysis of forced laminar convection heat transfer in the entrance region of an elliptical duct, *Int. J. Heat Mass Trans.* **16,** 1501–1503 (1973).
19. R. C. Dean, Jr. (Ed.), *Aerodynamic Measurements.* Massachusetts Institute of Technology Press, Cambridge, Mass. (1961).
20. J. Nikuradse, *Gesetzmassigkeit der Turbulenten Stromung in Glatten Rohren,* p. 356. Forschungsheft, Dusseldorf (1932).
21. R. M. Abdel-Wahed, A. E. Attia and M. A. Hifni, Error estimation in measuring temperature profiles for flow inside ducts, *Bull. Facl Engng, Alexandria Univ.* **XIX** (1) (1980).
22. S. T. McComas and E. R. G. Eckert, Laminar pressure drop associated with the continuum entrance region and for slip flow in a circular tube, *J. appl. Mech.,* ASME 87, Series E **32,** 765 (1965).
23. E. M. Sparrow, C. W. Hixon and D. Shavit, Experiments on laminar flow development in rectangular ducts, *Trans. ASME* **89,** 116 124 (1967).
24. H. Schlichting, *Boundary Layer Theory,* 4th Edn, p. 506. McGraw-Hill, New York (1960).


## APPENDIX

*Coefficients in equation* (5)

$\lambda_{1,0} = 14.97, \quad A_{1,0} = 0.88846$

| p/q | 1 | 3 | 5 | 7 | 9 |
|---|---|---|---|---|---|
| 0 | −0.9874 | 0.0152 | 0.0014 | 0.0003 | 0.0001 |
| 2 | 1.0000 | −0.0229 | −0.0020 | −0.0004 | −0.0001 |
| 4 | −0.2189 | 0.0094 | 0.0008 | 0.0002 | |
| 6 | 0.0312 | −0.0022 | −0.0002 | | |
| 8 | −0.0032 | 0.0003 | | | |
| 10 | 0.0003 | | | | |

$\lambda_{1,2} = 75.23, \quad A_{1,2} = 0.29624$

| p/q | 1 | 3 | 5 | 7 | 9 |
|---|---|---|---|---|---|
| 0 | −0.5831 | 0.0320 | −0.0001 | 0.0005 | 0.0004 |
| 2 | −0.4536 | −0.0211 | 0.0010 | 0.0007 | 0.0005 |
| 4 | 0.2132 | 0.0019 | −0.0020 | −0.0007 | −0.0003 |
| 6 | −0.0603 | 0.0005 | 0.0010 | −0.0005 | −0.0002 |
| 8 | 0.0024 | −0.0003 | −0.0005 | 0.0003 | |
| 10 | −0.0005 | −0.0003 | 0.0001 | | |
| 12 | 0.0002 | 0.0001 | | | |
| 14 | −0.0001 | | | | |

$\lambda_{3,0} = 106.4, \quad A_{3,0} = 0.19634$

| p/q | 1 | 3 | 5 | 7 | 9 | 11 |
|---|---|---|---|---|---|---|
| 0 | −0.1211 | −0.6312 | −0.0124 | −0.0112 | −0.0005 | −0.0002 |
| 2 | −0.1011 | −0.9694 | 0.0253 | 0.0186 | 0.0032 | 0.0001 |
| 4 | 0.0427 | 0.1663 | 0.0009 | −0.0097 | −0.0005 | |
| 6 | −0.0073 | −0.0673 | 0.0004 | 0.0003 | | |
| 8 | 0.0008 | 0.0053 | −0.0001 | | | |
| 10 | −0.0003 | −0.0002 | | | | |
| 12 | 0.0001 | | | | | |

## EXPERIENCES SUR L'ECOULEMENT LAMINAIRE ET SUR LE TRANSFERT THERMIQUE DANS UN TUBE ELLIPTIQUE

**Résumé**—Des expériences sont faites pour étudier l'écoulement laminaire en développement puis établi et le transfert thermique dans un tube elliptique avec un rapport d'axes de 0,5. Le fluide en mouvement est l'air et deux conditions thermiques sont considérées : la première avec le tube à température uniforme et l'autre avec une distribution pariétale de température linéaire dans la direction longitudinale et sans variation transversalement. Les résultats hydrodynamiques sont présentés sous forme d'une séquence de profils de vitesse sur les axes grand et petit, mesurés à différentes distances axiales depuis l'entrée du tube. La chute de pression statique due à l'effet combiné du développement de l'écoulement et du frottement pariétal est aussi étudiée. La longueur nécessaire au développement de la pression statique, exprimée par $x/Re\,D_h$, est 0,0345. L'information thermique dépeint le développement de la température à l'entrée du tube par une série de profils de température suivant les axes grand et petit. Les résultats concernent le nombre de Nusselt et la longueur d'établissement thermique pour chacune des conditions thermiques. D'après l'auteur, des solutions théoriques pour le développement hydrodynamiques n'existent pas pour les tubes elliptiques. Les présentes données expérimentales de régime établi sont comparées aux valeurs analytiques de Toa, pour les vitesses réduites et le coefficient de frottement. La différence pour ce dernier est de 0,78%. Le développement thermique a été étudié analytiquement par Dunwoody et Javeri pour une température pariétale respectivement uniforme et linéaire. Les deux analyses supposent un profil de vitesse soit uniforme, soit pleinement établi dans la région de développement du régime thermique.

## EXPERIMENTELLE UNTERSUCHUNG VON LAMINARER STRÖMUNG UND WÄRMEÜBERGANG IN EINEM ELLIPTISCHEN KANAL

**Zusammenfassung**—Die Ausbildung und der vollständig ausgebildete Zustand einer laminaren Luftströmung sowie der Wärmeübergang wurden in einem elliptischen Kanal (Achsenverhältnis 0,5) experimentell untersucht. Zwei Fälle wurden unterschieden : Im ersten hatte die Kanalwand eine einheitliche Temperatur, im zweiten war die Wandtemperaturverteilung in axialer Richtung linear und am Umfang konstant. Geschwindigkeits- und Temperaturprofile in Richtung der beiden Achsen wurden für verschiedene axiale Positionen dargestellt. Außerdem wurden Druckabfall, Nusselt-Zahl und Länge der thermischen Anlaufstrecke angegeben.

## ЭКСПЕРИМЕНТАЛЬНОЕ ИССЛЕДОВАНИЕ ЛАМИНАРНОГО ТЕЧЕНИЯ И ТЕПЛООБМЕНА В ЭЛЛИПТИЧЕСКОМ КАНАЛЕ

**Аннотация**—Проведено экспериментальное исследование развивающегося и полностью развитого ламинарного течения и теплопереноса внутри эллиптического канала с отношением полуосей 0.5. В качестве рабочей жидкости использовался воздух. Исследовались два случая: (1) равномерно нагретый канал и (2) канал с линейным распределением температуры стенки вдоль оси и постоянной температурой в поперечном направлении. Гидродинамические результаты представлены в виде последовательного ряда профилей скорости на большой и малой осях, измеренных на ряде участков по оси вдоль канала, начиная от входа в канал до области полностью развитого режима течения. Также рассматривается перепад статического давления по оси из-за совместного влияния динамики потока и трения на стенке. Найдено, что длина, необходимая для развития статического давления, определяемая отношением $x/ReD_h$ составляет 0.0345. Результаты по теплообмену представлены рядом температурных профилей на большой и малой осях эллиптического сечения, показывающих изменение температуры в области входа в канала. Эти результаты включают также число Нуссельта и длину теплового начального участка для каждого из указанных выше случаев. Насколько известно авторам, теоретические решения задачи развития гидродинамического течения на входе в эллиптические каналы отсутствуют. Представленные экспериментальные данные по полностью развитым безразмерным скорости и трению сравниваются с теоретическими значениями, полученными Л. М. Тоа. В процентном выражении различие в значениях коэффициента трения составляет 0.78%. Теплообмен при течении в эллиптическом канале изучался теоретически Н. Т. Данвиди и В. Джавери для равномерно нагретого канала и канала с линейным изменением температуры стенки. В обоих исследованиях предполагались или равномерные или полностью развитые профили скорости в режиме развитого течения.